RESEARCH ARTICLE

Engineering Thermoresponsive Emulsions with Branched Copolymer Surfactants

Marcelo Alves da Silva, Abhishek Rajbanshi, Daniel Opoku-Achampong, Najet Mahmoudi, Lionel Porcar, Philipp Gutfreund, Andrea Tummino, Armando Maestro, Cecile A. Dreiss, and Michael T. Cook*

This study describes thermo-rheological properties of branched copolymer surfactants (BCSs) stabilizing oil-in-water emulsions to generate materials exhibiting temperature-dependent gelation with the ability to solubilize a broad range of molecules. Four poly(N-isopropylacrylamide-*ran*-poly(ethylene glycol) methacrylate) (poly(NIPAM-*ran*-PEGMA)) BCSs with varying molecular weight (M_n), 4.7; 7.0; 7.8 and 9.0 kg mol^{-1}, are investigated via oscillatory shear rheology, small angle neutron scattering (SANS), and neutron reflectivity (NR). Rheological thermoscans show that emulsions stabilized by the BCS with the lowest M_n (4.7 kg mol^{-1}) are thermo-thinning, while with the other BCSs the emulsions display a thermo-thickening behavior. Emulsions stabilized with the BCS with M_n = 7.8 kg mol^{-1} form gels within a precise temperature window depending on BCS concentration. Small angle neutron scattering data analysis suggests that the BCS is present in two forms in equilibrium, small aggregates dispersed in the bulk water and an adsorbed polymeric layer at the oil/water interface. Changes in dimensions of these structures with temperature correlate with the macroscopic thermo-thinning/thermo-thickening behavior observed. Neutron reflectivity is conducted at the oil/water interface to allow further elucidation of BCS behavior in these systems.

1. Introduction

Emulsions are colloidal fluids composed of a mixture of immiscible liquids where one liquid is dispersed in a continuous phase of the other.[1,2] Emulsions are a ubiquitous everyday material found in food, paint, agrochemical and pharmaceutical industries.[1] This derives from their ability to combine two immiscible liquids, allowing the benefits from each liquid to be harnessed, for instance in the solubilization of incompatible substances. "Engineered emulsions", introduced by Weaver and co-workers,[3] provide a means to increase the functionality of emulsions by conferring them stimuli-responsiveness, that is, turning them into smart materials.[4–6] Creating a material that offers the solubilization potential of emulsions whilst responding to environment stimuli can bring together multiple advantages to yield highly functional materials with a broad range of applications.

An elegant approach to confer stimuli responsiveness to emulsions systems without

M. A. da Silva, A. Rajbanshi, D. Opoku-Achampong, M. T. Cook
School of Life and Medical Sciences
University of Hertfordshire
Hatfield, Hertfordshire AL10 9AB, UK
E-mail: m.cook5@herts.ac.uk

N. Mahmoudi
ISIS Neutron and Muon Source, STFC
Rutherford Appleton Laboratory
Didcot OX11 0QX, UK

L. Porcar, P. Gutfreund, A. Tummino
Institut Laue Langevin
71 Avenue des Martyrs, Grenoble 38042, France

A. Maestro
Centro de Fısica de Materiales (CSIC, UPV/EHU)
Materials Physics Center MPC
Paseo Manuel de Lardizabal 5, San Sebastián E-20018, Spain

A. Maestro
Ikerbasque
Basque Foundation for Science
Plaza Euskadi 5, Bilbao 48009, Spain

C. A. Dreiss
Institute of Pharmaceutical Science
King's College London
Franklin-Wilkins Building, 150 Stamford Street, London SE1 9NH, UK

**ADVANCED
SCIENCE NEWS**

www.advancedsciencenews.com

**Macro-
molecular
Materials and Engineering**

www.mame-journal.de

complex formulation of multiple components is to employ stimuli-responsive emulsifiers.[7] Emulsifiers are stabilizers used to prevent the dispersed phase in emulsions undergoing co-alescence and phase separation.[1] Emulsifiers, in general, are small surfactant molecules.[1] However, macromolecular sur-factants offer a degree of versatility not conferrable to small molecules.[5,7] Through the careful selection of the macromolec-ular constituents, it is possible to impart an amphiphilic char-acter to stimuli-responsive polymers.[8] For medical applications, thermo-thickening, an increase in viscosity upon heating, is a par-ticular useful property. A low viscosity fluid facilitates application, as the low viscosity allows an easier flow through, for example, a syringe or spray device, while a gel-like solid will improve reten-tion, localization and temporal stability.[9] Branched copolymer surfactants (BCSs)[8] have previously been demonstrated to im-part a pH-responsive behavior to emulsions,[7,8] allowing solidi-fication triggered by acidification, and thus offer a blueprint for the genesis of emulsions that respond to temperature.

BCSs may be generated via a scalable one-pot free-radical poly-merization, composing a feed mixture of "functional" monomer (i.e., leading to stimuli-responsive behavior in the copolymer), hy-drophilic monomer, cross-linker, and hydrophobic chain trans-fer agent (an alkyl thiol).[10] This approach is proposed herein for the generation of BCSs bearing thermoresponsive polymer chains grafted with hydrophilic blocks and terminated with hy-drophobic chain ends. This produces a macromolecule with both thermo-responsiveness and amphiphilic character. Poly-mers with a lower critical solution temperature (LCST), i.e., poly-mers that undergo phase-separation above a critical temperature, would be a crucial thermoresponsive component of the BCS, as their natural thermosensitivity can induce assembly processes and structural alterations within materials when heated. Poly(N-isopropylacrylamide) (PNIPAM) is a popular thermoresponsive polymer due to its water solubility and sharp, environmentally-insensitive LCST close to body temperature ($\approx$32 °C).[11,12] In prior study of thermoreversible gelators consisting of polymer so-lutions, the onset temperature for the thermoresponse and rhe-ological behavior are dependent on the nature of the thermore-sponsive polymer used and the architecture, which in turn dic-tates nanostructure and particle-particle interactions.[13] There-fore, the elucidation of the BCS nano-scale structures in these emulsions is necessary to produce engineered emulsions of high performance for specific applications.

This study probes the impact of the molecular weight of the BCS on its thermo-rheological behavior with the aim of generat-ing thermoresponsive engineered emulsions which solidify upon heating. To achieve this, the macroscopic thermo-rheological be-havior of the emulsions stabilized with these constructs will be investigated via shear oscillatory rheology. Small angle scatter-ing and neutron reflectivity are employed to characterize the nanoscale morphology of the BCS above and below the transition temperature. This approach enables the elucidation of nanoscale assembly processes which underpin thermoresponsive behavior in these engineered emulsions.

2. Results and Discussion

This work focused on studying thermally induced rheological transitions in BCS-stabilized emulsions with the aim of gen-erating thermo-thickening engineered emulsions. These BCSs were branched statistical copolymers bearing dodecyl chain-ends generated from a mixture of thermoresponsive and non-thermoresponsive polymers, illustrated in **Figure 1**. PNIPAM is the thermoresponsive component, exhibiting an LCST.[12] PNI-PAM undergoes a volume change transition at $\approx$32 °C, be-low which PNIPAM chains behave as they would in a good solvent, that is, as swollen coils, and above this transition as collapsed coils, as they would in a poor solvent. This volume change transition can then lead to (micro)phase separation of the PNIPAM component, triggering self-assembly processes in solution. Poly(ethylene glycol) methacrylate (PEGMA) provides a non-thermoresponsive component which is predominantly hy-drophilic at all temperatures studied and is anticipated to act as a steric stabilizer to the emulsions. Ethylene glycol dimethylacry-late (EGDMA) is included as a cross-linker to induce branch-ing, whilst 1-dodecanethiol (DDT) resides at chain termini to im-part hydrophobicity and is intended to anchor the BCS to the oil phase. These BCS were synthesized via radical polymerization at a PNIPAM:PEGMA:EGDMA ratio of 29:1:2 and characterized by GPC and ^{1}H NMR (Figures S1–S4, Supporting Information). The ratio of PNIPAM to PEGMA was set such that the NIPAM:EG ratio was 3:2, which gave the desired response in preliminary studies. Initial pilot studies with these BCSs demonstrated an ability to act as effective emulsifiers, whilst also imparting ther-moresponsive behavior, solidifying upon warming to form a ma-terial which did not flow under gravitational force (Figure 1b,c), demonstrating for the first time the formation of thermorespon-sive engineered emulsions stabilized by BCSs.

The impact of molecular weight on the behavior of thermore-sponsive engineered emulsions was probed by investigating a se-ries of four different BCS constructs with increasing M_n at dif-ferent concentrations. Control of M_n was achieved by increas-ing the ratio of monomer to DDT/AIBN, as described in the experimental section, thus the larger M_n also have a greater monomer:hydrophobic chain end (DDT) ratio. The effect of the monomer:hydrophobic chain end dependence on M_n is reflected on the BCS surface activity. The larger the M_n, the larger the crit-ical aggregation concentration (cac) measured (Figure S5, Sup-porting Information). The increase in M_n is achieved by elevat-ing the monomer (hydrophilic):chain end (hydrophobic) ratio. Thus, this also raises the overall hydrophilic character of the BCS, confirmed by the increase of the cac observed. Therefore a larger quantity of BCS is required before aggregates start to form. Dodecane-in-water emulsions were used as a model system as gelation relies on the interplay between the polymer construct and the dispersed oil phase. To specifically study the impact of polymer structure, the emulsions were kept to a minimal number of formulation parameters: BCS, water and oil. In order to enable a systematic analysis, emulsion preparation was standardized at a fixed 50:50 w/w water/oil content and a rest period of 1 week. The rest period was chosen to be long enough that no visible changes to the system were observed by eye after an initial creaming pe-riod. After this equilibration, the creamed phase was collected and the volume of the remaining water phase was measured. For the systems studied, the amount of remaining water phase was constant, $\approx$30% of the original mass, which was removed prior to experiments. The concentrations stated throughout the manuscript refer to the original preparation prior to creaming.
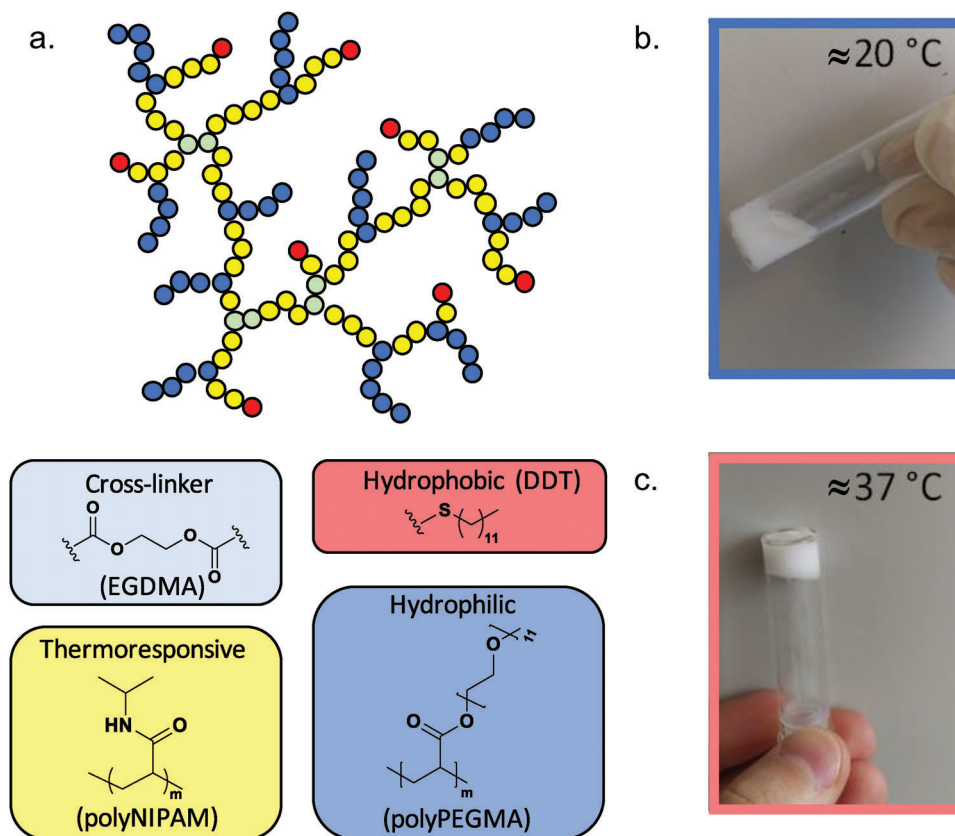
2200321 (2 of 14)

**ADVANCED
SCIENCE NEWS**

www.advancedsciencenews.com

**Macro-
olecular
Materials and Engineering**

www.mame-journal.de

Figure 1. Representation of BCS architecture formed from a single-pot synthesis, combining amphiphilicity with thermo-responsive behavior a). These BCS were found to form stable oil-in-water emulsions b) which solidified upon warming to body temperature c).

The resulting creamed phase has a high oil-content, greater than the original formulation, and saturated with BCS. A fraction of excess BCS was removed together with the excess water during isolation of the creamed phase.

Four BCS constructs with varying molecular weight were selected; for simplicity, they are named: Low M_n, Medium M_n, High M_n, and Very High M_n (corresponding to 4.7, 7.0, 7.8 and 9.0 kg mol^{-1}, respectively). One hypothesized mechanism for the sol–gel transition is that the BCSs can adsorb simultaneously on different droplets and, upon heating above the LCST, the PNIPAM block undergoes a volume change and stiff aggregates are formed, causing the oil droplets to jam, thus leading to a sudden increase in viscosity. Therefore, the intensity of the thermo-rheological behavior is expected to be dependent on the size (proportional to molecular weight) of the BCS.[14,15] Prior studies by Weaver and co-workers hypothesized that in pH-responsive emulsions, solidification is the result of inter-drop association by H-bonding of polymer at the surface to adjacent emulsion droplets.[3,16,17] This concept of droplet-droplet interaction informed this initial paradigm for solidification.

Rheological evaluation was conducted on BCS-stabilized emulsions to monitor temperature-induced phenomena. Rheological thermoscans of the four BCS-stabilized emulsions with three different BCS concentrations are shown in **Figure 2**. The graphs show the dependence of the storage (G′) and loss (G″) moduli with the temperature. G′ (also referred to as the elas-tic modulus) relates to the elastic part of the shear deformation, while G″ (also referred to as the viscous modulus) relates to the dissipative part of the shear deformation. Thus, the magnitude of G′ and G″ provide information on the "thickness" of the system while their ratio relates to how solid-like or liquid-like the material behaves. For this work, the G′ and G″ cross-over point is taken as the gelation point.[18]

Thermoscans for all the four poly(NIPAM-*ran*-PEGMA) BCS-stabilized emulsions were conducted (Figure 2). For the Low M_n BCS investigated, both G′ and G″ experience a small decrease above the transition temperature, ≈35 °C, indicating a thermo-thinning behavior. The magnitude of the thermo-thinning behavior is dependent on polymer concentration: G′ dropped 33% at 1.25 wt% BCS compared to a 68% drop at 2.5 wt% BCS, and a 77% drop at 5.0 wt% BCS, comparing G′ at 25 and 50 °C. This change takes place across the temperature at which a volume-change transition is observed for PNIPAM.[12] Increasing M_n from low (4.7 kg mol^{-1}) to medium (7.0 kg mol^{-1}) leads to a dramatic behavior change. Emulsions stabilized by this Med M_n poly(NIPAM-*ran*-PEGMA) show a clear thermo-thickening behavior starting at a slightly lower temperature, ≈32 °C, but no actual gelation is observed as G′ remains lower than G″; however, a thickened emulsion is produced within a narrow range of temperatures, with both moduli increasing, and the systems thinning as the temperature rises above ≈40 °C. Emulsions with High and Very High M_n poly(NIPAM-*ran*-PEGMA) behave in

ADVANCED
SCIENCE NEWS
www.advancedsciencenews.com

[M] acro-
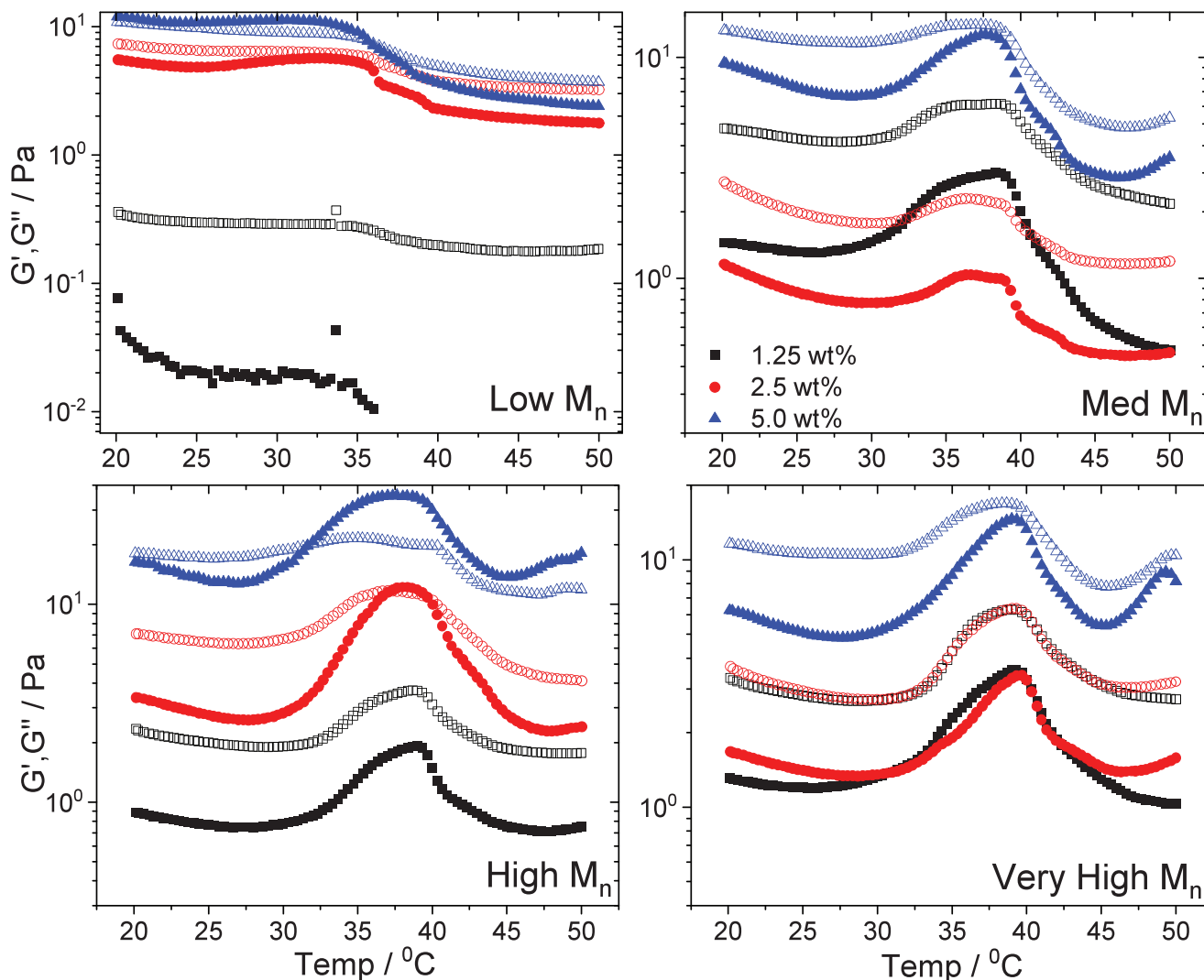molecular
Materials and Engineering
www.mame-journal.de

Figure 2. Shear oscillatory measurements showing the rheological dependence of BCS-stabilized emulsions with temperature for Low M_n, Medium M_n, High M_n and Very High M_n BCS, at 1.25, 2.5 and 5.0 wt%. G': closed square symbols, G'': open circle symbols.

a similar manner. Gelation is obtained for emulsions with high M_n (7.8 kg mol^{-1}), 5.0 wt% BCS, with G' overcoming G'', but is not observed for the Very High BCS (9.0 kg mol^{-1}) systems. The magnitude of the thermo-thickening is also concentration dependent with the highest concentration presented, 5.0 wt%, showing the largest effect. This indicates that the thermo-rheological behavior is tied to molecular weight and polymer concentration, and that there is an optimal chain length for gelation to occur. All emulsions were visually inspected after a heat-cool cycle and no further phase separation was observed, which confirmed that the emulsions were still stable. A second thickening event can be also seen in Medium, High and Very High M_n BCS systems (**Figures** 2 and **3**) starting ≈45 °C. This event is related to the BCS present in the bulk water, discussed later in the manuscript (**Figure 4**).

The thermo-rheological response observed is not always reversible over short-time scales as can be observed in Figure 3, which shows cooling down as a featureless returning curve, except for High M_n BCS, where a weak gel region is observed between 35 and 32 °C during cooling.

In Figure 4, thermoscans of aqueous solutions of Low and High M_n BCS are presented. No thickening is observed in the 35 °C region for High M_n BCS, confirming that the thermo-thickening observed in the emulsions is due to an interaction between the polymer and the dispersed oil droplets. However, the second thickening event observed in the emulsions at ≈45 °C is clearly observed. Thus, this second event is hypothesized to arise from BCS behavior in water and not be related to BCS-oil droplet interactions, making the BCS solutions interesting thermoresponsive materials in their own right. It is expected for the LCST of PNIPAM in BCS to increase due to the presence of the hydrophilic copolymer[6,19] and shows an important role of the non-LCST polymer in shifting the onset of BCS phase separation.
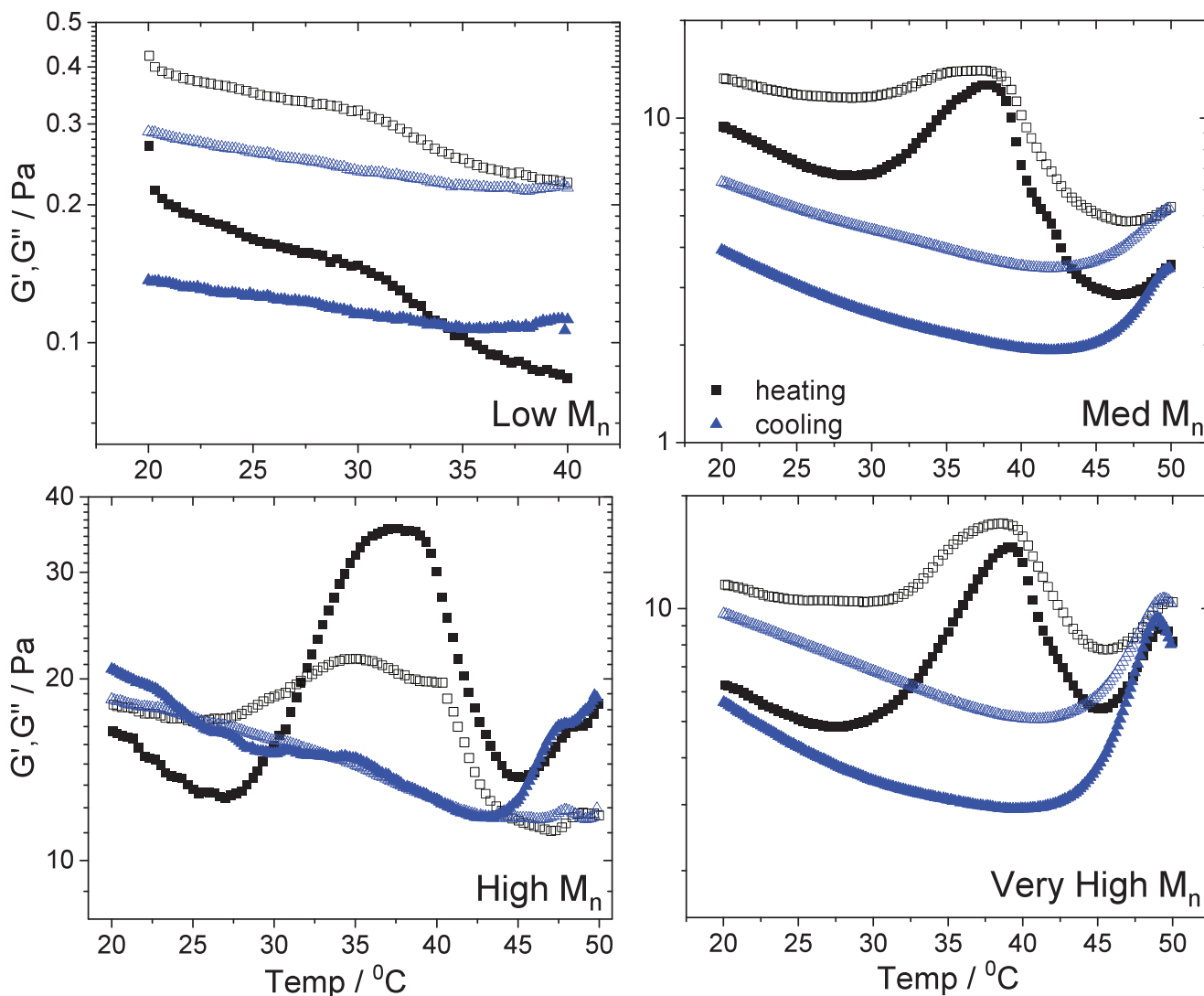
**ADVANCED
SCIENCE NEWS**

www.advancedsciencenews.com

[M] acro-
olecular
Materials and Engineering

www.mame-journal.de

Figure 3. Shear oscillatory measurements showing the rheological response of 5.0 wt% BCS stabilized emulsions to a single heat-cool cycle for Low M_n, Medium M_n, High M_n, and Very High M_n BCS. G': closed square symbols, G'': open circle symbols.

SANS data were collected for BCS emulsions (**Figure 5**) and solutions (Figure 7) to probe the BCS behavior at nanometer length-scales. The emulsions studied were prepared using D_2O as the water phase and a mixture of 95 wt% d_{26}-dodecane and 5.0 wt% h_{26}-dodecane to match the SLD of D_2O; for simplicity, these emulsions are denoted as "D_2O/d-dodecane". This results in a system where both the water and oil phases have the same scattering length densities (SLD). Therefore, the SLD contrast dominating the scattering is due to BCS versus water/oil with negligible scattering arising from the water/oil interface. Two other contrasts were studied, "H_2O/d-dodecane", where the scattering arises from the BCS present in the oil phase and in the water phase, the stronger contribution being from the BCS in the oil phase (BCS estimated SLD = 0.54×10^{-6} Å^{-2} versus d-dodecane SLD = 6.707×10^{-6} Å^{-2})[20] (Figure S6, Supporting Information) plus a contribution from the oil/water interface itself. The third contrast was "D_2O/h-dodecane", where the opposite is observed,

scattering from BCS present in the water and in the oil phase will be observed but the dominant signal should arise from the BCS in D_2O, plus a contribution from the water/oil interface (Figure S7, Supporting Information). The H_2O/d-dodecane contrast set showed little sensitivity to temperature or BCS M_n, and the data can be satisfactorily fitted with a single power law following an exponent equal to -4 showing that the dominant signal arises from the oil/water interface and was not further investigated.

The SANS data were collected at four different temperatures, below the transition, 25 °C, around the transition, 37 °C and 40 °C, and above the transition, 50 °C. This temperature range covers both transitions observed in the rheograms (Figures 2 and 4). At 37 °C, the thermal transition due the changes in the emulsion dominates, at 50 °C, the BCS thermal transition in the bulk water phase dominates, while at 40 °C, we expect both events to be important. For all the four systems studied, the data at 25 °C were adequately fitted using a power law+sphere model (**Table 1**).
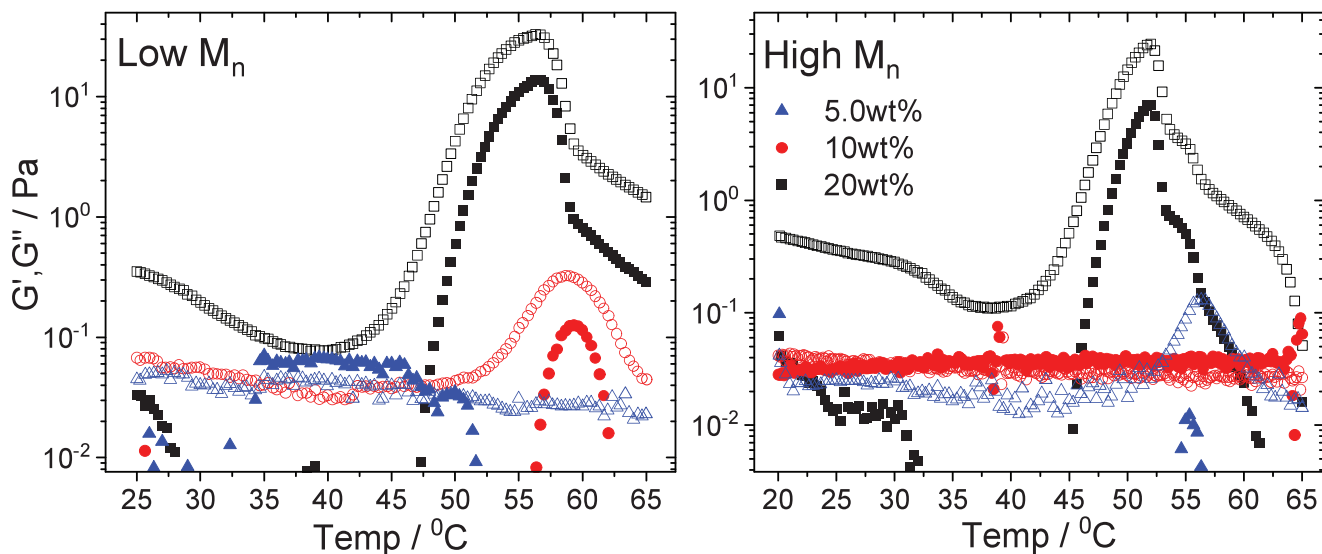
**ADVANCED
SCIENCE NEWS**

www.advancedsciencenews.com

[M]acro-
molecular
Materials and Engineering

www.mame-journal.de

Figure 4. Shear oscillatory measurements showing the rheological dependence of BCS aqueous solutions with temperature for Low M_n and High M_n BCS. G′: closed square symbols, G″: open circle symbols.

The spherical contribution is thought to arise from polymeric aggregates. The power law likely reflects the presence of larger structures formed from further assembly of the aggregates. The power law exponent changes from −2.8 for Low M_n to −3.6 for Very High M_n (Table 1). Assuming the presence of fractal aggregates, this shows an evolution from volume (exponent between −2 and −3) to surface fractals (−3 to −4):[21] an evolution from open to more condensed structures. The radii of these spherical aggregates varies only slightly with the different polymers, from 42 ± 1 (Low M_n) to 39 ± 1 Å (Very High M_n).

The SANS data above the transition were fitted using a combination of a sphere model (representing BCS aggregates) combined to an infinite isotropic flat layer (**Table 2**),[22–24] representing the build-up of polymer at the droplet interface. Studies on microgel stabilized Pickering emulsions have shown that soft PNIPAM microgels pack densely and spread over an oil/water interface depending on the softness of the microgel.[25,26] A similar behavior can be expected from PNIPAM based-BCS, as the BCS does not have a high degree of internal crosslinking, only branching, and therefore would be more deformable than microgels. For the emulsions studied here, the droplet sizes are in the micrometer range, 2.5 to 11 μm (Figure S8, Supporting Information) and highly polydisperse; therefore, they can be considered as an infinite flat layer at the SANS length scale. The scattering data from the third contrast, D$_2$O/h-dodecane, was satisfactorily fitted using the data obtained for the D$_2$O/d-dodecane dataset plus a fixed power law contribution of −4 and was not further investigated (Figure S7, Supporting Information).

The spherical aggregates grow as temperature increases and a sharp increase is observed from 40 to 50 °C. Low and Medium M_n BCS generated larger aggregates at 50 °C than High and Very High M_n BCSs, for example, the radius for Low M_n BCS aggregates at 50 °C is 223 ± 1 Å versus 128 ± 1 Å for High M_n BCSs. The thickness of the BCS layer at the interface follows a different trend. For Low M_n BCS, the layer thickness decreases with temperature. For the Med to VHigh Mn, the layer thickness remains

relatively stable from 37 to 40 °C and increases from 40 to 50 °C. At 50 °C, Medium M_n shows a thicker layer than High and Very High M_n, 91 Å versus 55 and 65 Å, respectively.

With regards to the rheological response, the BCS can be divided into two groups: thermo-thinning (Low M_n), and thermo-thickening (Med, High and Very High M_n). The SANS data broadly suggest the same grouping, based on the size of the aggregates and thickness of the adsorbed layer, with some similarity with Low M_n and Med M_n only at the highest temperature. While these behaviors alone do not provide a complete mechanism for the thermoresponse, the data show that dimensional stability of both layer and aggregates are important for the thermo-thickening transition: emulsions stabilized with Low M_n BCS— the system displaying thermo-thinning—also show the largest variations in dimensions, with a collapse of layer thickness with temperature, and a very large increase in the size of the aggregates (Table 2).

The data also highlights the contributions of the two thermal events observed. At circa 35 °C, thermo-thinning or thermo-thickening is observed (Figure 3) and this event only happens in emulsion systems (Figure 4), namely, the emulsion thermoresponse. At circa 45 °C a thermo-thickening event is observed (Figures 3 and 4), and it is present in both emulsions and aqueous solutions. This second event will lead to phase separation in solution as the temperature increases (Figure S9, Supporting Information). The data suggest that the second thermal event involves a large growth of the BCS aggregates present in the water phase, especially at the oil/water interface. During coalescence and phase separation such behavior would be expected where BCS aggregation leads to overall larger structures. This might be also causing the irreversibility of the emulsion thermoresponse (Figure 3), as the BCS aggregates strongly, it may be locked in a configuration that is unsuitable for the emulsion thermoresponse. This also would explain the narrow temperature window that the thermo-thickening is observed within. As the temperature increases, the BCS-BCS aggregation becomes more
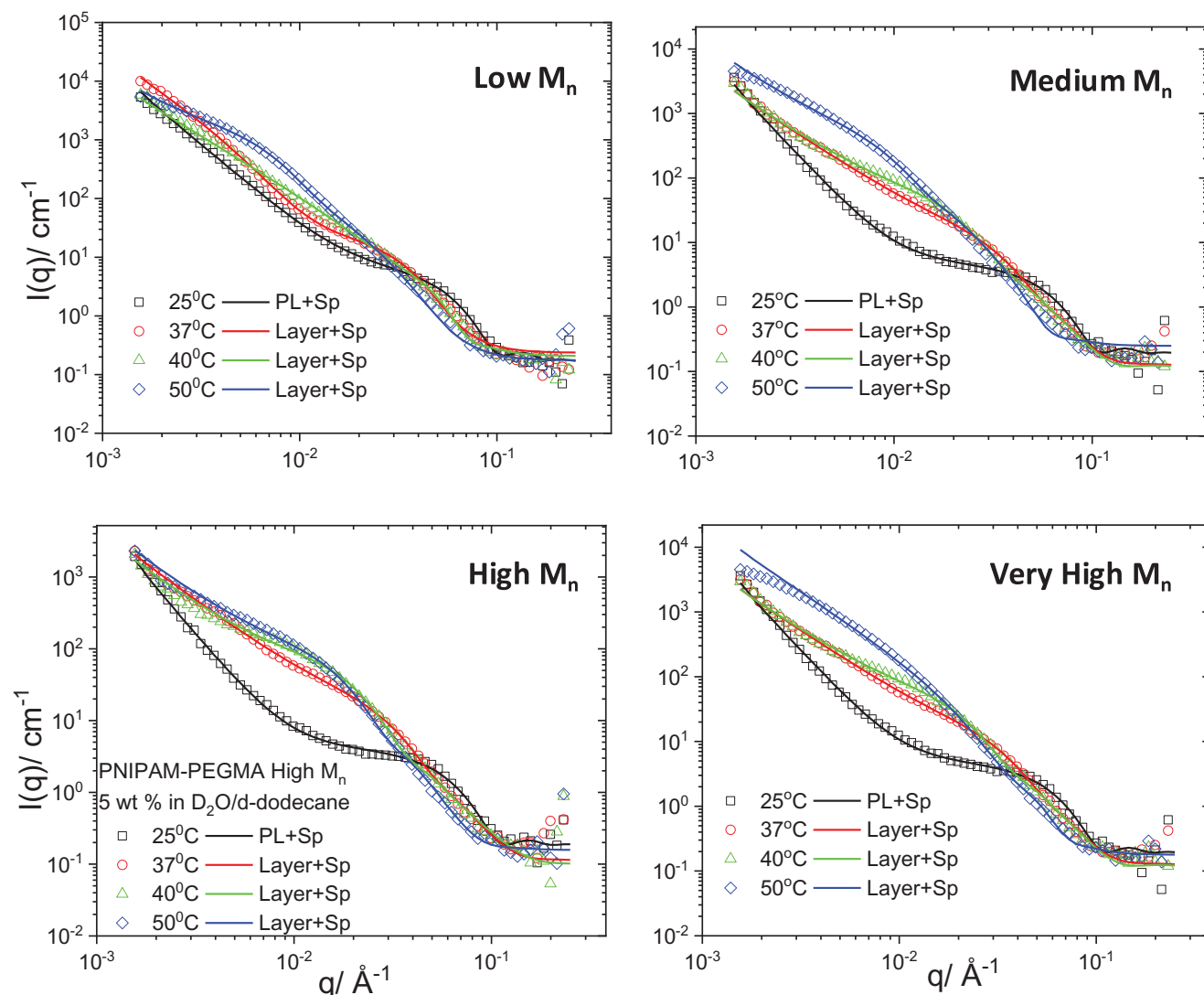
![ADVANCED SCIENCE NEWS]
www.advancedsciencenews.com

[M] acro-molecular
Materials and Engineering
www.mame-journal.de

Figure 5. SANS curves and fits for 5.0 wt% BCS-stabilized emulsions at different temperatures (25, 37, 40, and 50 °C) for Low M_n, Medium M_n, High M_n and Very High M_n BCS in D_2O/d-dodecane. PL+Sp = power law and sphere models. Layer+Sp = infinite thick layer+sphere model.

Table 1. Results from the SANS analysis of BCS-stabilized emulsions below transition temperature (25 °C), using a power law+sphere model.

BCS [M_n]	Radius [Å]	Power law
Low	42 ± 1	2.8 ± 0.2
Med	39 ± 1	3.2 ± 0.2
High	38 ± 1	3.2 ± 0.2
Very High	39 ± 1	3.6 ± 0.2

important leading to a competition between the two processes where the phase separation dominates. Therefore, an ideal BCS would preserve the thermoresponse at ≈35 °C while delaying the phase separation to higher temperatures minimizing the overlap of the two events.

The current hypothesized model for the emulsion thermoresponse is that BCS polymeric chains that form the aggregates can participate in more than one aggregate and also be adsorbed to the water/oil interface.[7,15] This leads to the formation of a connected network of BCS aggregates and oil droplets. At the transition temperature, PNIPAM blocks in the BCS collapse, causing the aggregates and droplets to agglomerate, thus "jamming" the system, and leading to thickening and gel formation. A priori, the BCS M_n would directly affect the network connectivity; if the BCS chains are too short, inter-polymer connections are likely to be more limited. The SANS data shown here suggest that the size evolution of BCS aggregates with temperature is also important: BCS aggregates growing too large with temperature seems to hinder the thickening process, for example, Low M_n aggregates growing in size from 38 to 223 ± 1 Å as the temperature increases from 37 to 50 °C, versus High M_n, where the radius changes from 73 to 128 ± 1 Å over the same temperature range. The data also shows the importance of oil/water layer configuration, as the only thermo-thinning BCS, Low M_n, also shows a very thick layer, at 37 °C, the Low M_n is ≈10x thicker

**ADVANCED
SCIENCE NEWS**
www.advancedsciencenews.com

Macromolecular
Materials and Engineering
www.mame-journal.de

Table 2. Results from the SANS analysis of BCS-stabilized emulsions above the transition temperature (37, 40 and 50 °C).

Temp 37 °C		
BCS M_n	Layer thickness [Å]	Radius [Å]
Low	441	38
Med	41	66
High	32	73
Very High	33	66

Temp 40 °C		
BCS [M_n]	Layer thickness [Å]	Radius [Å]
Low	153	51
Med	38	105
High	30	104
Very High	33	84

Temp 50 °C		
BCS M_n	Layer thickness [Å]	Radius [Å]
Low	92	223
Med	91	244
High	55	128
Very High	65	131

Data were fitted using an infinite layer+sphere model. The error-bar on lengths is estimated to ±1 Å.

than the other BCSs. Previous study of PNIPAM-graft-PEGMA stabilized emulsions attributed increases in viscosity to flocculation, however this was not macroscopically observed in these BCS systems and SANS did not evidence random flocculation events.[7,27] Large aggregates and a thicker layer may hamper the gel connectivity, as a dispersion of numerous small objects facilitates interconnectivity while a reduced number of larger objects are likely to remain isolated. One clue for the likely reason for the Low M_n BCS generating larger aggregates might be reflected by its surface activity. As discussed previously, the larger the M_n, the greater the monomer:hydrophobic chain end (DDT) ratio, therefore, the less hydrophobic the BCS. Surface tension measurements confirm (Figure S5, Supporting Information) this behavior, the larger the M_n, the higher the cac. The initial assumption is that below the cac, the BCS will be in an equilibrium between chains at the interface and dispersed in the bulk water, as the BCS is a water soluble polymer, a larger presence in water is expected and the higher the cac, the higher this presence. The more hydrophobic Low M_n BCS is more likely to adsorb into the interface, generating thicker layers, and while producing less water dispersed aggregates, and the aggregates generated would be larger than the Higher M_n, to minimize solvent exposure. Both the factors contribute to less connectivity throughout the system. The higher M_n, due the higher hydrophilicity, will have a greater concentration of single chains in solution and, as SANS shows, smaller aggregates, which favors interconnectivity.

Neutron reflectivity (NR) was used to directly probe the oil/water interface of BCS/water/oil mixtures to model the emul-

sion system. Historically, NR has focused on solid–liquid interfaces, but a newer method allows NR studies of these more-relevant liquid-liquid interfaces.[28] The BCS is added to the water phase and no energy is added to the system, unlike in the process required to produce the emulsions, where high energy homogenization is required. In this measurement, only one flat macro interface is present. Perfluorooctane (PFO) was used instead of dodecane, as it has high cold neutrons transmittivity, differently from alkanes,[28] and an SLD distinct from the alkyl end chains and the BCS polymeric backbone, creating a good contrast between BCS and the oil phase to ensure signal in this challenging experimental set-up. PFO also has a higher density than D_2O, and therefore will remain at the bottom of the reflectivity measurement cell. High and Low M_n constructs were measured in D_2O/PFO at 25, 35 and 45 °C for High M_n, and 25 and 35 °C for Low M_n (**Figure 6**). Experimental data at the fully accessible q-range were collected and analyzed using a one-layer model of constant SLD, which would correspond to a BCS layer in contact with both bulk phases and modulated by a Gaussian error function accounting for the respective interfacial roughness (see Section 4 for further details). In contrast to SANS, a polymer layer is detectable at 25 °C for both systems (**Table 3**). In the data at 35 °C, no difference in layer thickness is observed, where both Low and High M_n BCS produce a layer of similar thickness. Low M_n BCS generates layers slightly more hydrated and with lower roughness at the oil interface than High M_n BCS. At 45 °C, thickening of the BCS layer is seen in the High M_n system measured, in broad agreement with SANS studies on the emulsions.

SANS data were also collected for BCS solutions in D_2O (**Figure 7**) to provide insights on the self-assembly behavior of the BCS in solution. The data below the transition temperature (25 °C) were fitted using a Guinier–Porod model.[29] This model combines a generalized form of the Guinier model with a power law and provides a radius of gyration and a dimension variable that describes the shape of the scattering object with a power law exponent for the high-q range (**Table 4**). The Porod exponent was fixed at 4 for all systems, reflecting a sharp interface. The dimension variable changes as follows: 2 (Low M_n), 1 (Med M_n), 1 (High M_n) and 0 (Very High M_n) (Table 4).

Above the transition temperature (40 and 50 °C), the data were fitted using two-Lorentzian distributions; this model provides a characteristic length of the scattering object and an exponent that carries information about the scattering object morphology (**Table 5**).[21] The smaller length, $\approx$20–40 Å has an associated –4 exponent. This suggests objects with sharp interfaces, interpreted as micelle-like aggregates. The larger length scale, $\approx$98 to 248 ± 1 Å, shows a range of exponents from −3.6 to 4.0 (Table 5). As observed for the emulsions, the largest length scale observed is for the Low M_n, 248 ± 1 Å at 40 °C and the value falls to 157 ± 1 Å at 50 °C. For the other BCS, both lengths increase with temperature, for example, from 75 to 115 ± 1 Å for High M_n BCS from 40 to 50 °C (for the longer dimension, length 1) and 21 to 61 ± 1 Å for the shorter dimension (length 2).

The solution SANS data above the transition temperature can be interpreted as larger aggregates (longer length) formed by smaller aggregates (shorter length). The forward scattering intensity, $I(q = 0)$, carries information about the size and number of scatterers. For Low and Med M_n BCS, a drop of $I(q = 0)$ is observed, while for High and VHigh M_n an increase is
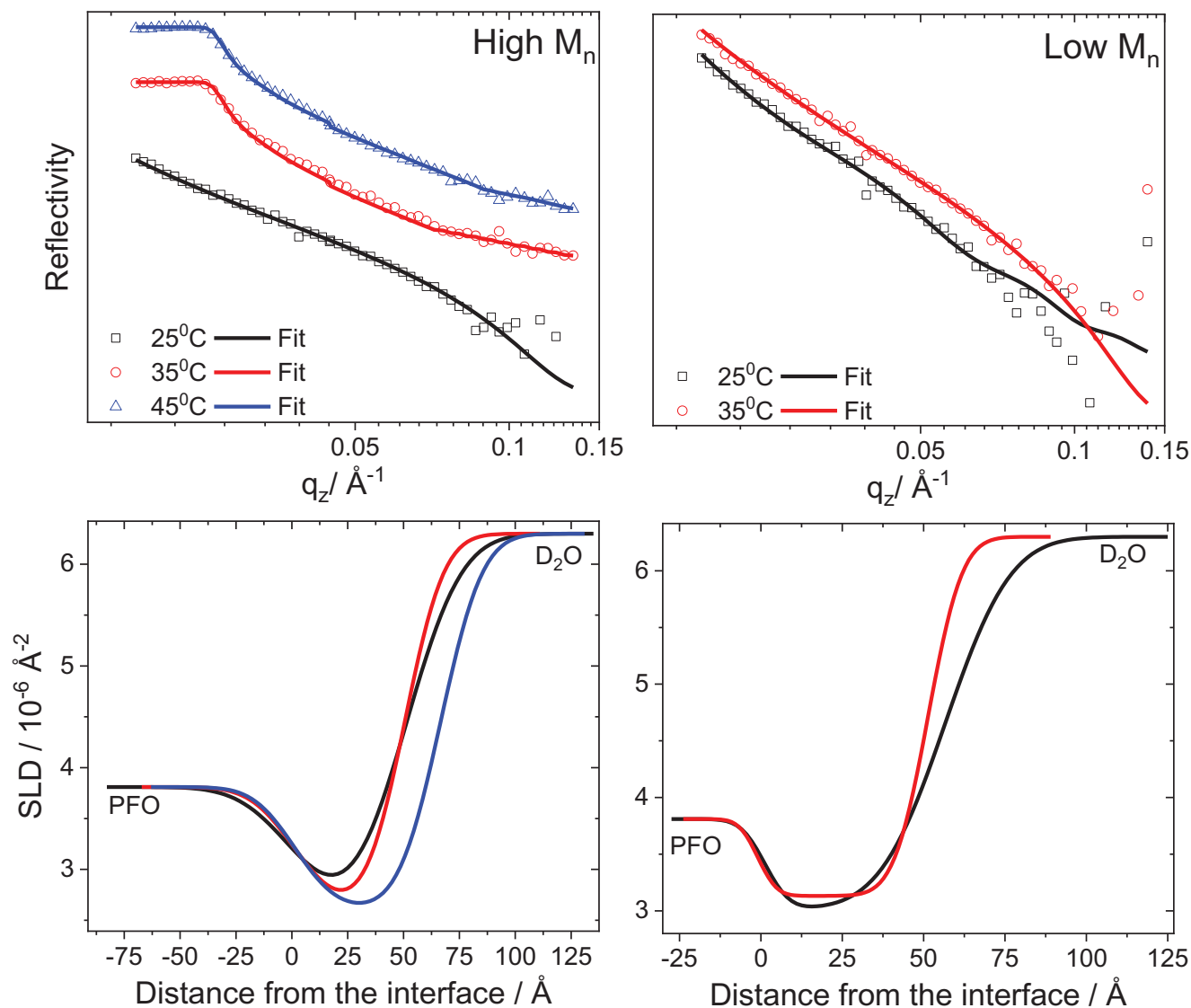
ADVANCED
SCIENCE NEWS

www.advancedsciencenews.com

{M} acro-
molecular
Materials and Engineering

www.mame-journal.de

Figure 6. (Top) Stacked neutron reflectivity profiles for High M_n and Low M_n PNIPAM-PEGMA BCS dispersions at D_2O/PFO interface at different temperatures. Solid lines are fits to the data. (Bottom) Corresponding SLD profiles for High M_n and Low M_n PNIPAM-PEGMA BCS dispersions.

Table 3. Neutron reflectivity fitting parameters for BCS High and Low M_n for D_2O/PFO systems.

BCS High M_n

Temp [°C]	Layer thickness [Å]	Layer hydration [%]	Water/layer roughness [Å]	Oil/layer roughness [Å]
25	50 ± 15	34 ± 3	20 ± 3	20 ± 3
35	50 ± 15	36 ± 3	16 ± 3	14 ± 3
45	66 ± 15	36 ± 3	15 ± 3	15 ± 3

Low M_n

Temp [°C]	Layer thickness [Å]	Layer hydration [%]	Water/layer roughness [Å]	Oil/layer roughness [Å]
25	56 ± 15	43 ± 3	16 ± 3	6 ± 3
35	57 ± 15	45 ± 3	9 ± 3	5 ± 3

**ADVANCED
SCIENCE NEWS**

www.advancedsciencenews.com

**[M] acro-
molecular
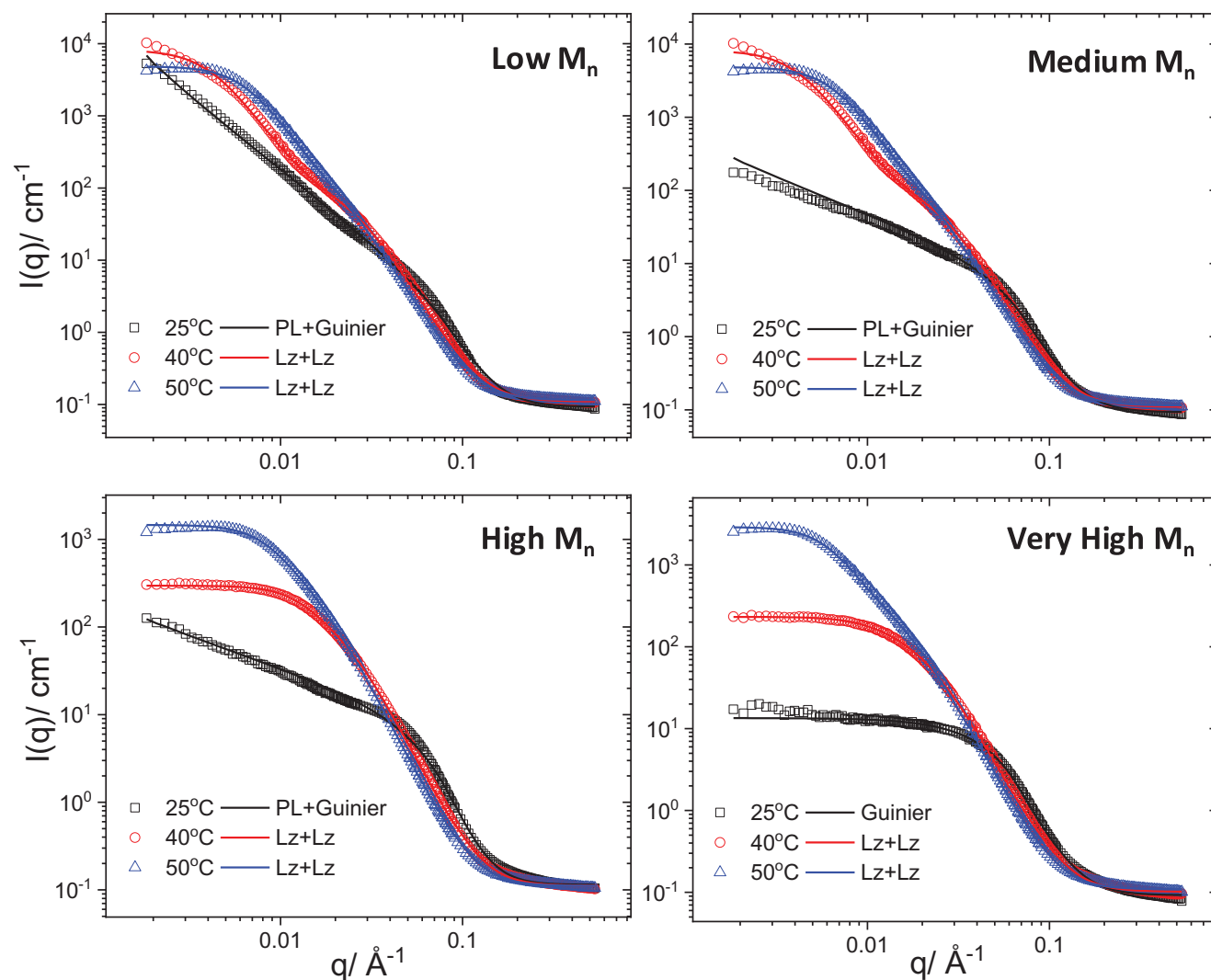Materials and Engineering**

www.mame-journal.de

Figure 7. Small angle neutron scattering curves and fits for 5.0 wt% BCS dispersions at different temperatures for Low, Medium, High and Very High M_n BCS. PL+Guinier = power law + generalized Guinier model. Lz+Lz = Lorentzian+Lorentzian model.

Table 4. Results from the SANS analysis for BCS D_2O solutions below the transition temperature (25 °C).

	BCS			
	Low M_n	Med M_n	High M_n	Very High M_n
Radius of gyration [Å]	11 ± 1	23 ± 1	21 ± 1	36 ± 1
Dimension variable	2(fixed)	1(fixed)	1(fixed)	0(fixed)
Porod exponent	4(fixed)	4(fixed)	4(fixed)	4(fixed)

Data were fitted using a power law combined to a Guinier–Porod model. Dimension variables: sphere = 0, rods = 1 and lamellae = 2.

Table 5. Results from the SANS analysis for BCS D_2O solutions above the transition temperature (40 and 50 °C).

BCS	Low M_n		Med M_n		High M_n		Very High M_n	
Temp [°C] ± 0.1	40.0	50.0	40.0	50.0	40.0	50.0	40.0	50.0
Length 1 [Å] ± 1	248	157	98	253	75	115	85	162
Exponent 1 ± 0.3	3.6	3.8	3.7	3.6	4.0	4.0	3.6	4.1
Length 2 [Å] ± 1	39	46	42	71	21	61	47	62
Exponent 2 ± 0.3	4.1	4.1	4.0	3.9	4.0	4.0	4.0	4.0
I (q = 0) [cm^{-1}]	7800	4600	7400	4800	300	1500	230	3000

Data were fitted using two Lorentzian-type models.

observed, instead. Also Low and Med shows larger I(q = 0) values than High and VHigh M_n BCS. That suggests that Low and Med forms large aggregates at 40 °C which break down a 50 °C, while High and VHigh form smaller aggregates at 40 °C that grow at 50 °C. For all BCS, the main change upon transition should be the temperature-induced volume-change of the PNIPAM block,

leading to a shrinkage of the polymer chain. The increase in dimensions observed suggests an aggregation process for the High and Very High M_n constructs, while the distinct behavior of the Low and Med M_n polymer is interpreted as a loss of connectivity

**ADVANCED
SCIENCE NEWS**

www.advancedsciencenews.com

{M}acro-
molecular
Materials and Engineering

www.mame-journal.de

within the larger aggregate, leading to its breakdown. This is attributed to the smaller size of the polymer chains in the BCS itself.

Taking the data for the thermo-thickening systems (Medium, High, Very High M_n) as a whole, the following conclusions are drawn:

- Two thermo-thickening events are observed by rheology. The first is associated with gelation (G' > G'') in concentrated systems and occurs around 35 °C, close to PNIPAM LCST; the second at ≈45 °C involves an increase in viscosity whilst the emulsions remain predominantly liquid-like (G'' > G'). Rheological measurements of the polymer solutions confirm that only the event at 45 °C is a result of polymer–polymer associations, while interactions between polymer and droplets are necessary for the event at 35 °C.
- SANS analysis of thermo-thickening emulsions shows the presence of spherical nanoscale aggregates across the temperature range, which grow in size during heating. Below the LCST, this aggregation is attributed to the association of hydrophobic alkyl chain ends. Above the LCST, they are likely to arise due to the association of PNIPAM, enabling further aggregation into larger particulates. This hypothesis is supported by SANS on solutions of the BCSs, which indicate the presence of two structures with different length scales: one small structure (≈20–50 Å radius) and a larger structure (≈75–250 Å radius), which could arise from the association of the smaller particles.
- Both neutron reflectivity and SANS measurements detect the presence of polymer at the oil–water interface, with polymer chains predominantly in the aqueous phase. The thickness of this layer increases with temperature, indicating associations between polymer at the interface and in the bulk as temperature rises past the LCST transition
- The overlapping of emulsion thermoresponse and the BCS phase separation reduces the temperature range where BCS-stabilized emulsions gels can form.

Taking these observations into account, the thermo-thickening event at ≈35 °C is attributed to an LCST type transition, taking place both at the interface and in the bulk. This leads to a clustering of polymer aggregates in solution which associate with polymer at the oil–water interface, leading to the percolating network responsible for gel formation (**Figure 8**).

Thermo-thinning emulsions obtained with the Low M_n BCS show, after an initial aggregation event, a reduction in the size of the polymer layer at the interface concomitant with a large increase of the BCS aggregates. In contrast, the BCS with higher molecular weights forms stable and finer layers and larger aggregates within the temperature of the first thickening event (32–45 °C). This could be attributed to the greater potential for longer polymer chains to overlap and consolidate physical interactions to retain elastic interactions in the system in the bulk water, leading to a better connected network of aggregates and the thinner layer being better anchored or more densely packed at the interface than the thicker but more prone to shrinkage layer observed in the Low M_n case.

3. Conclusion

This work reports the generation of thermoresponsive engineered emulsions. The thermo-responsive behavior of emulsions stabilized by branched copolymer surfactants at the macro (rheology) and nanoscale (SANS and NR) is described. The BCS are branched copolymers of NIPAM and PEGMA with hydrophobic dodecyl end groups. Above a transition temperature (the LCST), at ≈32 °C, PNIPAM undergoes a transition from a swollen to a collapsed coil, which leads the emulsion either to thin or thicken with increasing temperature, a behavior that is dependent upon the molecular weight. Four BCS of varying molecular were investigated, namely, Low (4.7 kg mol^{-1}), Medium (7.0 kg mol^{-1}), High (7.8 kg mol^{-1}) and Very High (9.0 kg mol^{-1}) M_n. These four BCS were selected to evaluate the impact of molecular weight on the thermo-rheological behavior of BCS-stabilized emulsions. Rheological data show that the Low M_n thins above the transition temperature, while the other three BCS thicken, irreversibly in most cases. A second thickening event is observed at a higher temperature, ≈45–50 °C, associated with the BCS phase separation. SANS and NR data suggest the formation of a BCS layer at the oil/water interface and the presence of BCS micelle-like aggregates in the aqueous phase. The SANS and NR data show that in emulsions stabilized with the thermo-thinning Low M_n, the BCS layer at the interface thins as temperature increases while the size of the micelle-like aggregates increases substantially with temperature. For the three thermo-thickening BCS, the BCS layer at the oil/water interface is relatively stable in between 37 and 40 °C and aggregates grow in size as temperature increases. This supports a mechanism of gelation where BCS-BCS and BCS-droplet aggregation above the LCST drives network formation in the system.

4. Experimental Section

Materials: *N*-Isopropylacrylamide (NIPAM, 97%), ethylene glycol dimethacrylate (EGDMA, 98%, contains 90–110 ppm monomethyl ether hydroquinone as inhibitor), poly(ethylene glycol) methyl ether methacrylate (PEGMA, average M_n 950 kg mol^{-1}, contains 300 ppm BHT as inhibitor, 100 ppm MEHQ as inhibitor), 1-dodecanethiol (DDT, ≥98%), 2,2′-azobis(2-methylpropionitrile) (AIBN, 98%) and deuterium oxide (99.9 atom % D) were purchased from Merck Life Science UK Limited (UK). *N*-dodecane-d26 was purchased from Qmx Laboratories (UK). Perfluorooctane (99%) was purchased from Abcr GmbH (DE). Ethanol (absolute) was purchased from Fisher Scientific (UK). All chemicals were used as received and without further purification. Deionized water was used throughout the experiments. Dialysis tubing cellulose membrane (molecular weight cut-off = 14000 g mol^{-1}) was purchased from Merck Life Science (UK).

Branched Copolymer Surfactant Synthesis by Radical Polymerization: Poly(*N*-isopropylacrylamide)-*ran*-poly(ethylene glycol) methacrylate branched copolymer surfactants (BCSs) were synthesized following a modified procedure outlined by Weaver et al. for the synthesis of pH-responsive BCSs.[3] NIPAM (19.7 mg, 174 mmol), PEGMA (5.7 g, 6 mmol), EGMA (2.39 g, 12 mmol) were solubilized in 190 mL ethanol. DDT was then added with quantity dependent on the final BCS molecular weight. For this study, four BCS with different molecular weights were synthesized: Low, Medium, High and Very High molecular weight. The amount of DDT added for each synthesis was 2.43 g (12 mmol), 1.62 g (8 mmol), 1.21 g (6 mmol) and 0.607 g (3 mmol), respectively. The solution was flushed with nitrogen for one hour. Afterwards, a 10 mL ethanol solution of AIBN was added. The AIBN amount was dependent on the final molecular weight desired. For Low, Medium, High and Very
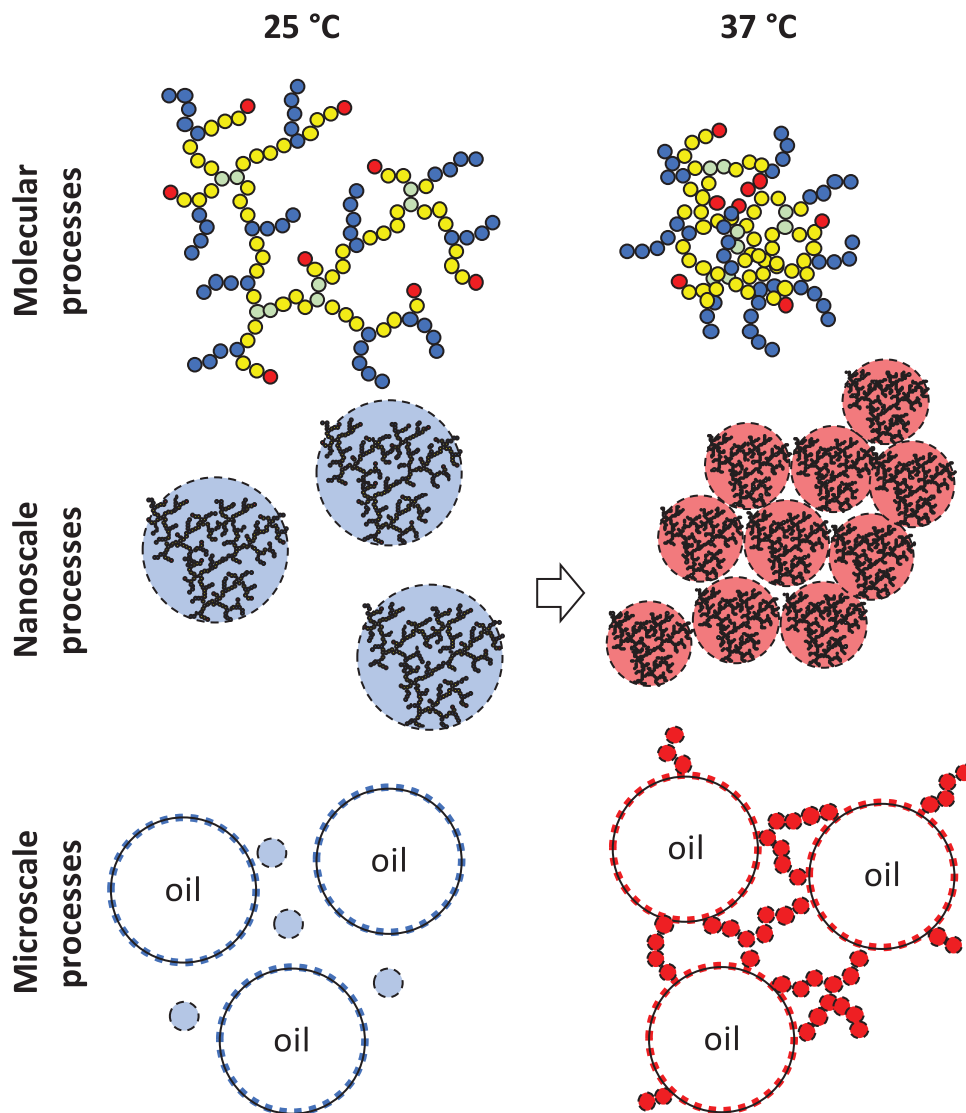
**ADVANCED
SCIENCE NEWS**

www.advancedsciencenews.com

$\left[\text{M}\right]$ acro-
molecular
Materials and **Engineering**

www.mame-journal.de

Figure 8. Proposed mechanism of gelation in thermo-thickening engineered emulsions. PNIPAM collapse above the LCST leads to polymer–polymer interactions, inducing clustering of BCS aggregates. In emulsion systems, these polymer–polymer interactions also occur between nanoaggregates in the bulk and polymer at the interface, forming elastically active bridges.

High the AIBN added was 197 mg (1.2 mmol), 131 mg (0.8 mmol), 98.5 mg (0.6 mmol) and 49.3 mg (0.3 mmol), respectively, retaining a 1:10 stoichiometry with the DDT chain transfer agent, but modifying monomer feed ratio. The reaction was then allowed to proceed for 48 h at 70 °C. Afterward, ethanol was distilled off the reaction mixture until it was concentrated to $\approx$50 mL. At this stage, aliquots were collected for NMR for determination of monomer conversion. The reaction media was then mixed with 50 mL deionized (DI) water and dialyzed against DI water for 7 days. The dialyzed BCS solution was freeze-dried and the dry BCS was recovered. The yields for the polymers used in this work are as follows: Low—60%, Medium—52%, High—53% and Very High—68%). Yield calculated as mass ratio of product over total mass of initial reagents.

Polymer Characterization: BCS were characterized using ^{1}H NMR in CDCl$_3$ on a Jeol ECA 600 MHz instrument at room temperature. The residual solvent peak was used as an internal standard. Spectra were processed using Delta 5.3.1 NMR software (Figures S1–S4, Supporting Information).

Number-average molecular weight (M_n) and polydispersity (Đ) was measured by gel permeation chromatography (GPC) employing an Agilent

12600 Infinity II GPC instrument equipped with a refractive index detector. The GPC used 2 × Varian PLGel 5 μm mixed-D columns which were run in sequence. Dimethylformamide with 0.1% lithium bromide was the eluent, running at a flow rate of 0.4 mL min^{-1} with the columns and detector held at 30 °C. The GPC was calibrated with Agilent Easivial poly(methyl methacrylate) standards with M_n ranging from 370 to 364 000 Da. The obtained M_n were as follows: LM$_n$ – Mn = 4.7×10^3 g mol^{-1} (Đ:1.86), MM$_n$ – M_n = 7.0×10^3 g mol^{-1} (Đ:2.26), HM$_n$ – M_n = 7.9×10^3 g mol^{-1} (Đ:2.09) and VHM$_n$ – M_n = 9.0×10^3 g mol^{-1} (Đ:2.21). The ratio of NIPAM to EG was calculated by ^{1}H NMR from the N$\underline{H}$ proton of NIPAM (4.0 ppm) and the OC$\underline{H}_3$ of PEGMA (3.4 ppm), giving 1.5:1, 1.5:1, 1.3:1 and 1.5:1 for the LM$_n$, MM$_n$, HM$_n$ and VHM$_n$, respectively. Surface tension measurements of aqueous BCS dispersions was conducted at room temperature employing a Torsion balance (Model OS -Torsion Balance Supplies, UK) equipped with a platinum Du Nouy ring (circumference of 4 cm) to determine critical aggregation concentrations (Figure S5, Supporting Information).

Rheological Measurements: Temperature scans were conducted on a TA AR 1500 ex shear rheometer equipped with a Peltier temperature

control unit using a 40 mm steel parallel plate geometry. The scans were conducted at fixed angular frequency of 6.28 rad s^{-1} and strain of 1%. The BCS emulsion was heated from 20 to 50 °C at a heating rate of 1 °C min^{-1}. A solvent trap was used to prevent evaporation during the experiment.

Small Angle Neutron Scattering (SANS) of BCS Solutions and BCS-Stabilized Emulsions: BCS solution SANS experiments were performed on the D11 instrument at the Institut Laue-Langevin (Grenoble, France). The neutron wavelength was set to 6 Å, the sample-detector distance at 2, 5.6, and 17.6 m, with a collimation distance of 2.8, 8, and 17.6 m, respectively. The detector offset was 300 mm. These settings resulted in a wave vector range $2.7 \times 10^{-3} \leq q \leq 0.45$ Å^{-1}. Rectangular quartz cuvettes with a thickness of 1 mm were used for all samples. Measurements were performed at 25, 40, and 50 °C with a minimum equilibration time of 15 min prior to sample run.[30] Data reduction and treatment was performed on GRASP, stitching was performed on Igor Pro (Wavemetrics, USA)[31] and data fitting was conducted using SasView 4.2.2.[32]

SANS experiments covering the BCS-stabilized emulsions were conducted on the time-of-flight diffractometer instrument SANS2d at the STFC ISIS Neutron and Muon Source (UK).[33] Incidental wavelengths from 1.75 to 12.5 Å were used with a sample-to-detector distance of 12 m, corresponding to a total scattering vector range q from 1.6×10^{-3} to 0.25 Å^{-1}. The sample temperature was controlled by an external circulating thermal bath (Julabo, DE). The scattering intensity was converted to the differential scattering cross-section in absolute units using ISIS standard procedures.[34] Samples were loaded in 1 mm path length, 1 cm wide optical rectangular quartz cells.[35] Contrast match experiments were done at 100 wt% D_2O/95 wt% d-dodecane-5.0 wt% h-dodecane, which matches both oil and water, in 100 wt% D_2O/100 wt% h-dodecane and in 100 wt% H_2O/100 wt% d-dodecane. SANS data were fitted using SASView 4.2.2.[32] The scattering length densities (SLDs) were calculated from the monomeric unit using the Neutron activation and scattering calculator website from NIST center for neutron research (Neutron activation and scattering calculator).[36]

The scattering intensity I(q) can be written as follows:

$$I(q) = A \left(P(q)_A S(q)_A \right) + BKG \tag{1}$$

where:

A is a proportionality constant,
BKG is the background,
$P(q)_A$ is the form factor of the scattering object,
$S(q)_A$ is the corresponding structure factor.

If more than one scattering object is present or the object studied has a hierarchical structure that generates scattering at distinct length scales, the expression can be extended to include further terms.

For this work, the polymer constructs, in general, give rise to two scattering signals, one arising from its supramolecular structures and the other from the polymeric chains. Therefore, I(q) is expressed as:

$$I(q) = A \left(P(q)_A S(q)_A \right) + B \left(P(q)_B \right) + BKG \tag{2}$$

where:

A and *B* are proportionality constants,
BKG is the background,
$P(q)_A$ is the form factor for model A,
$S(q)_A$ is the corresponding structure factor,
$P(q)_B$ is the form factor for model B.

Emulsion data models A and B were either a combination of power law[37]+sphere model,[38] below the transition temperature, or lyotropic lamellar phase with uniform SLD and random distribution (infinite thick layer)[39]+sphere model,[38] above the transition temperature. Solution data were fitted either using a Guinier+Porod[29] model or double-Lorenztian model.[37]

Neutron Reflectivity (NR): Neutron reflectivity experiments were conducted at the Institut Laue-Langevin (France) using the Fluid Interfaces Grazing Angles Reflectometer (FIGARO).[40] The reflectivity R(q$_z$) was measured using the time-of-flight technique as a function of momentum transfer normal to the interface $q_z = (4\pi \sin \theta)/\lambda$, where θ is the grazing angle of incidence of neutrons with wavelength λ. The neutron reflectivity profiles were measured at incident angles of $\theta = 0.67°$ and $1.4°$ ($\lambda = $ 2.2–20 Å) providing a wide q$_z$ range. The sample was under-illuminated with a constant resolution $\delta Q/Q \approx 7\%$. The background around the specular reflection peak was subtracted using the 2D detector on FIGARO.[41] Measurements were conducted at 23, 37 and 45 °C for poly(NIPAM-*ran*-PEGMA) High M$_n$ in D_2O/PFO and 23 and 37 °C for poly(NIPAM-*ran*-PEGMA) Low M$_n$ in D_2O.

A liquid/liquid cell made in quartz was used for the experiments. A description of the cell design optimized for both reflections up/down modes in FIGARO minimizing neutron attenuation can be found elsewhere.[28] Here, it was connected to a syringe pump to control the injection of the bulk phases as well as to align the oil/water interface with respect to the neutron beam. Data modelling was performed by minimizing the difference between the experimental and the calculated reflectivity profile. The latter was obtained by a model consisting of one layer of constant SLD (= 0.54×10^{-6} Å^{-2}) using the Parratt's recursive formalism,[42] with an error function connecting the layer with the each of the two bulk phases (D_2O and PFO) that describes the corresponding interfacial roughness. Parameters defining the layer (thickness, roughness, and water volume fraction) were optimized during the fitting procedure using Motofit.[43] The hydration of the layer defined as the volume fraction of the aqueous phase $f_w \phi 1 - \phi_{BCS}$ was calculated as follows: $SLD_{fit} = SLD_{BCS}\phi_{BCS} + SLD_w\phi_w$.

Supporting Information

Supporting Information is available from the Wiley Online Library or from the author.

Conflict of Interest

The authors declare no conflict of interest.

Data Availability Statement

The data that support the findings of this study are available from the corresponding author upon reasonable request.

[1] F. Adams, P. Walstra, B. W. Brooks, H. N. Richmond, M. Zerfa, J. Bibette, D. J. Hibberd, M. M. Robins, J. G. Weers, A. S. Kabalnov, D. N. Petsev, T. Obey, B. Vincent, H. Kunieda, R. Pons, C. Solans, T. H. Forster, W. Von Rybinski, P. Smulders, T. Iwanaga, B. Deminiere, A. Colin, F. Calderon, *Modern Aspects of Emulsion Science*, The Royal Society of Chemistry, London **1998**.

[2] D. H. Everett, *Pure Appl. Chem.* **1972**, *31*, 577.

[3] J. V. M. Weaver, S. P. Rannard, A. I. Cooper, *Angew. Chem., Int. Ed.* **2009**, *48*, 2131.

[4] G. Pasparakis, M. Vamvakaki, *Polym. Chem.* **2011**, *2*, 1234.

[5] M. A. C. Stuart, W. T. S. Huck, J. Genzer, M. Müller, C. Ober, M. Stamm, G. B. Sukhorukov, I. Szleifer, V. V. Tsukruk, M. Urban, F. Winnik, S. Zauscher, I. Luzinov, S. Minko, *Nat. Mater.* **2010**, *9*, 101.

[6] M. T. Cook, P. Haddow, S. B. Kirton, W. J. McAuley, *Adv. Funct. Mater.* **2021**, *31*, 2008123.

[7] A. Y. C. Koh, B. R. Saunders, *Chem. Commun.* **2000**, *6*, 2461.

[8] R. T. Woodward, R. A. Slater, S. Higgins, S. P. Rannard, A. I. Cooper, B. J. L. Royles, P. H. Findlay, J. V. M. Weaver, *Chem. Commun.* **2009**, 3554.

[9] M. T. Cook, M. B. Brown, *J. Controlled Release* **2018**, *270*, 145.

[10] R. Baudry, D. C. Sherrington, *Macromolecules* **2006**, *39*, 1455.

[11] F. Doberenz, K. Zeng, C. Willems, K. Zhang, T. Groth, *J. Mater. Chem. B* **2020**, *8*, 607.

[12] S. Lanzalaco, E. Armelin, *Gels* **2017**, *3*, 36.

[13] M. A. Da Silva, P. Haddow, S. B. Kirton, W. J. Mcauley, L. Porcar, C. A. Dreiss, M. T. Cook, *Adv. Funct. Mater.* **2021**, *32*, 2109010.

[14] C. Alava, B. R. Saunders, *J. Colloid Interface Sci.* **2006**, *293*, 93.

[15] A. Y. C. Koh, B. R. Saunders, *Langmuir* **2005**, *21*, 6734.

[16] R. T. Woodward, J. V. M. Weaver, *Polym. Chem.* **2011**, *2*, 403.

[17] J. V. M. Weaver, S. P. Rannard, A. I. Cooper, *Angew. Chem.* **2009**, *121*, 2165.

[18] M. A. Da Silva, I. A. Farhat, E. P. G. Arêas, J. R. Mitchell, *Biopolymers* **2006**, *83*, 443.

[19] P. Chambon, L. Chen, S. Furzeland, D. Atkins, J. V. M. Weaver, D. J. Adams, *Polym. Chem.* **2011**, *2*, 941.

[20] Neutron activation and scattering calculator.

[21] S. M. King, in *Modern Techniques for Polymer Characterisation* (Eds: R. A. Pethrick, J. V. Dawkins), John Wiley & Sons, Ltd, Chichester **1999**, pp. 171.

[22] B. Yesiltas, M. Torkkeli, L. Almásy, Z. Dudás, A. F. Wacha, R. Dalgliesh, P. J. García-Moreno, A.-D. M. Sørensen, C. Jacobsen, M. Knaapila, *J. Colloid Interface Sci.* **2019**, *554*, 183.

[23] P. A. Reynolds, E. P. Gilbert, J. W. White, B. Yesiltas, M. Torkkeli, L. Almásy, Z. Dudás, A. F. Wacha, R. Dalgliesh, P. J. García-Moreno, A.-D. M. Sørensen, *J. Phys. Chem. B* **2000**, *104*, 7012.

[24] P. A. Reynolds, D. J. Mcgillivray, J. P. Mata, P. N. Yaron, J. W. White, *J. Colloid Interface Sci.* **2010**, *349*, 544.

[25] M. Destribats, V. Lapeyre, M. Wolfs, E. Sellier, F. Leal-Calderon, V. Ravaine, V. Schmitt, *Soft Matter* **2011**, *7*, 7689.

[26] Z. Li, K. Geisel, W. Richtering, T. Ngai, *Soft Matter* **2013**, *9*, 9939.

[27] A. Y. C. Koh, C. Prestidge, I. Ametov, B. R. Saunders, *Phys. Chem. Chem. Phys.* **2002**, *4*, 96.

[28] E. Scoppola, S. Micciulla, L. Kuhrts, A. Maestro, R. A. Campbell, O. V. Konovalov, G. Fragneto, E. Schneck, *Molecules* **2019**, *24*, 4113.

[29] B. Hammouda, *J. Appl. Crystallogr.* **2010**, *43*, 716.

[30] M. T. Cook, M. A. da Silva, C. A. Dreiss, L. Porcar, Engineering thermoresponsive branched copolymer surfactants: Influence of the copolymer composition on thermoresponse.

[31] S. R. Kline, *J. Appl. Crystallogr.* **2006**, *39*, 895.

[32] SasView version 4.2.2.

[33] R. K. Heenan, S. E. Rogers, D. Turner, A. E. Terry, J. Treadgold, S. M. King, *Neutron News* **2011**, *22*, 19.

[34] ISIS SANS Data Reduction in Mantid.

[35] M. T. Cook, A. Rajbanshi, C. A. Dreiss, N. Mahmoudi, M. A. da Silva, Engineering emulsions from thermoresponsive branched copolymer surfactants: Influence of the copolymer composition on thermoresponse.

[36] Neutron activation and scattering calculator.

[37] O. Glatter, O. Kratky, *Small Angle X-ray Scattering*, Academic Press, London; New York **1982**.

[38] A. Guinier, G. Fournet, *Small-Angle Scattering of X-Rays*, University Microfilms International, Ann Arbor, MI; London **1979**.

[39] F. Nallet, R. Laversanne, D. Roux, *J. Phys. II* **1993**, *3*, 487.

[40] R. A. Campbell, H. P. Wacklin, I. Sutton, R. Cubitt, G. Fragneto, *Eur. Phys. J. Plus* **2011**, *126*, 107.

[41] P. Gutfreund, T. Saerbeck, M. A. Gonzalez, E. Pellegrini, M. Laver, C. Dewhurst, R. Cubitt, *J. Appl. Crystallogr.* **2018**, *51*, 606.

[42] L. G. Parratt, *Phys. Rev.* **1954**, *95*, 359.

[43] A. Nelson, *J. Appl. Crystallogr.* **2006**, *39*, 273.